

Instrument Signature Removal and Calibration Products for the Rubin Legacy Survey of Space and Time

Andrés A. Plazas Malagón^{a,b,*}, Chris Waters^d, Alex Broughton^c, Eli Rykoff^{a, b}, Agnès Ferté^{a,b}, Merlin Fisher-Levine^e, Robert Lupton^d

^aSLAC National Accelerator Laboratory, Menlo Park, CA, USA

^bKavli Institute for Particle Astrophysics and Cosmology, Stanford University, Stanford, CA, USA

^cDepartment of Physics and Astronomy, University of California-Irvine, Irvine, California, USA 92617

^dDepartment of Astrophysical Sciences, Princeton University, Princeton, NJ, USA

^eRubin Observatory Project Office, 950 N. Cherry Ave., Tucson, AZ, USA

Abstract. The Vera C. Rubin Legacy Survey of Space and Time (LSST) will conduct an unprecedented optical survey of the southern sky, imaging the entire available sky every few nights for 10 years. To achieve its ambitious science goals of probing dark energy and dark matter, mapping the Milky Way, and exploring the transient optical sky, the systematic errors in the LSST data must be exquisitely controlled. Instrument signature removal (ISR) is a critical early step in LSST data processing to remove inherent camera effects from the raw images and produce accurate representations of the incoming light. This paper describes the current state of the ISR pipelines implemented in the LSST Science Pipelines software. The key steps in ISR are outlined and the process of generating and verifying the necessary calibration products to carry out ISR is also discussed. Finally, an overview is given of how the Rubin data management system utilizes a data Butler and calibration collections to organize datasets and match images to appropriate calibrations during processing. Precise ISR will be essential to realize the potential of LSST to revolutionize astrophysics.

Keywords: CCDs, algorithms, software, calibration, galaxy surveys.

*Andrés A. Plazas Malagón, plazas@slac.stanford.edu

1 Introduction

The Vera C. Rubin Observatory, currently under construction on Cerro Pachón in Chile, will undertake the Legacy Survey of Space and Time (LSST) using the state-of-the-art Simonyi Survey Telescope. With an 8.4-meter primary mirror and a 3.2-gigapixel camera (LSSTCam), the LSST aims to conduct an unprecedented survey of over 18,000 square degrees of the southern sky using six different filters spanning the optical and near-infrared spectrum. The LSST has four main science goals: probing dark energy and dark matter, creating an inventory of the solar system, exploring the transient optical sky, and inferring the structure and evolution of the Milky Way galaxy.¹ To achieve these goals, the LSST area will be observed more than 800 in 10 years.

To attain the precision necessary for these ambitious science goals, the systematic errors in the LSST data must be exquisitely controlled. The raw data from the camera contain inherent instrument signatures from effects like bias levels, dark current, and amplifier noise. Instrument signature removal (ISR) is a critical early step in LSST data processing, aimed at removing these camera-induced effects to produce accurate representations of the incoming light. This process includes using specific calibration images and corrections to eliminate the instrument's effects from the raw data.

The focal plane of the LSSTCam consists of 189 thick (100 microns), fully-depleted, back-illuminated science Charge-Coupled Devices (CCDs),²⁻⁴ in addition to 8 CCDs for guiding and 4 split CCDs for wavefront measurements.^{5,6} The science CCDs are arranged in 21 rafts, each powering and controlling nine CCDs. Each CCD is divided into sixteen segments, each with

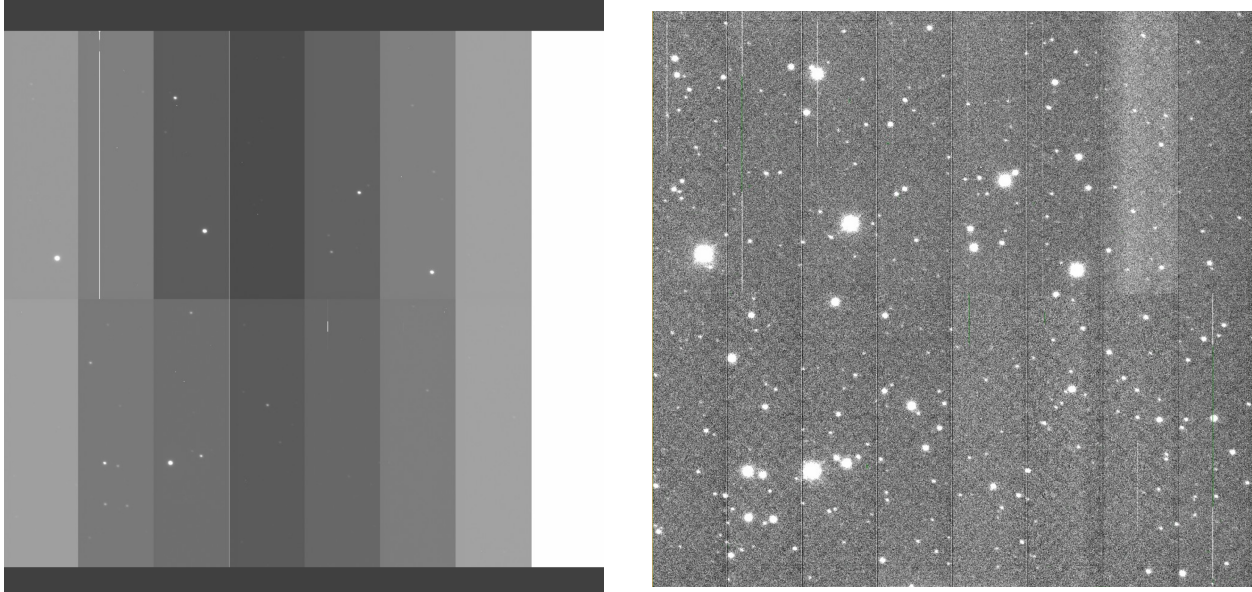


Fig 1 Example of an image before and after partial Instrument Signature Removal (bias, dark, and flat applied).

a separate readout register and amplifier, for low-noise, fast parallel readout, resulting in 3024 image segments for the science detectors. The LSSTCam focal plane contains CCDs fabricated by two vendors, the ITL STA3800C from the University of Arizona Imaging Technology Laboratory (ITL),^{7 1} and the E2V CCD250 from Teledyne E2V.² With 201 CCDs in the camera, ISR for LSST is a challenging task.

This paper is structured as follows: Section 2 describes the steps in ISR currently implemented in the LSST Science Pipelines^{8,9} codebase, including steps planned for future development. Section 3 describes the generation, construction, and verification process of the necessary calibrations for ISR in the LSST. Section 4 concludes with a general description of the Rubin data management paradigm and how the pipelines are constructed and executed.

2 Instrument Signature Removal for the LSST

Figure 1 shows an example of an image before and after partial ISR processing, with applied bias, dark, and flat-field images. The full sequence of ISR steps to go from a raw image in Analog-to-Digital Units (ADU) to a post-ISR image in e^- is displayed in Figure 2 and presented in the following subsections, including steps not yet implemented in our pipelines (in red and dashed in Figure 2 and signaled with an asterisk in the subsection title). This is the status of the current ISR algorithms as of version `w_2024_13` of the LSST Science Pipelines.³

2.1 Input validation

The ISR task receives as input *raw*, unassembled images in Analog-to-Digital (ADU) units. The task then validates that it has the necessary input calibration files to perform the requested ISR steps in the task configuration file.

¹<https://www.itl.arizona.edu/>

²<https://www.teledyneimaging.com/en/aerospace-and-defense/products/sensors-overview/ccd/ccd250-82/>

³The ISR code can be found at https://github.com/lsst/ip_isr

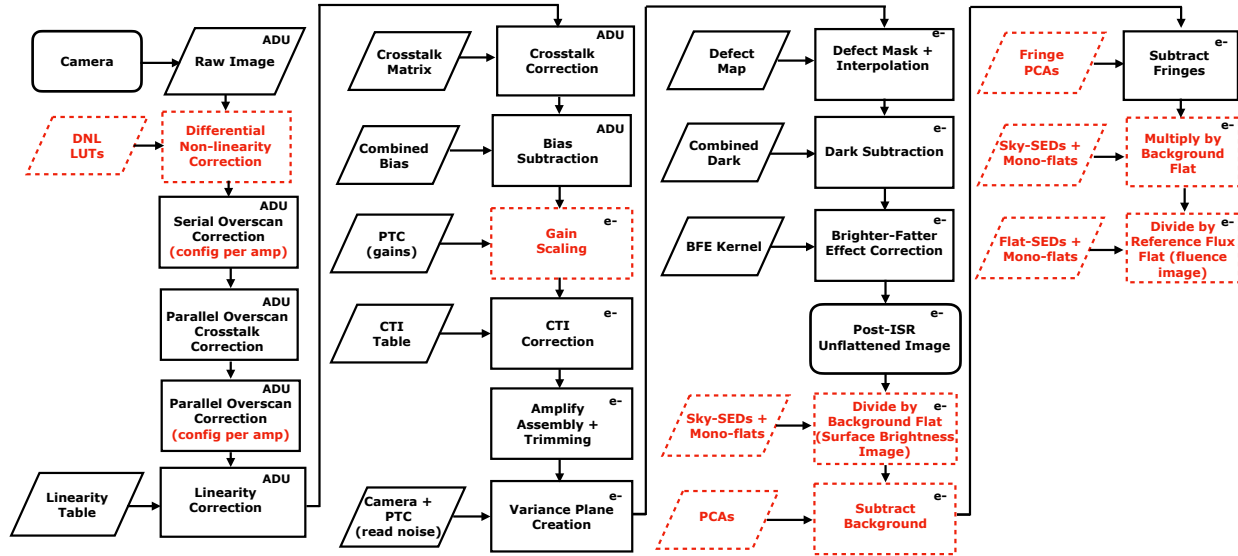


Fig 2 ISR steps and necessary calibration products. Units are displayed in each box, and the steps in red and enclosed in dashed lines are in the process of being implemented. Flowchart based on discussions at Rubin Calibration Workshop at SLAC, October 2023.

2.2 Differential non-linearity correction*

Differential non-linearity (DNL) in the CCD analog-to-digital converter (ADC) occurs when there is a bias toward the digital output values (0 or 1). Ideally, no ADC levels should be “narrow” or “wide”. To incorporate DNL correction into the ISR pipelines, correction algorithms can be defined to generate look-up tables for each potential signal level in ADU.

2.3 Correction of the serial overscan

The ISR task performs a serial overscan correction (the overscan being extra readouts of the serial register after a row has been read out) to remove amplifier bias levels, which may be unstable with time. For LSSTCam, the routine is set to define the overscan correction as the population median per row (`MEDIAN_PER_ROW`), but other correction options are available (e.g., via the mean of the overscan region or spline fits). The first three columns of the overscan are skipped to mitigate the impact of deferred charges (the number of columns to skip is configurable).

As with other ISR steps, future versions of the code will allow this process to be configured per detector and amplifier.

2.4 Bad amplifier and SATURATED/SUSPECT pixel masking

After serial overscan correction, pixels flagged as `SATURATED` and `SUSPECT` are masked. The appropriate definition of saturation is still under consideration. Potential definitions include the mean pixel full-well, the Photon-Transfer Curve (PTC¹⁰) turnoff, the level at which serial or parallel Charge Transfer Inefficiency (CTI) exceeds requirements, the maximum observed level in a given pixel, and the level at which detectors exhibit significant persistence.¹¹

2.5 Correction of the crosstalk from the image to the parallel overscan region and parallel overscan correction

For certain amplifiers, parallel overscan subtraction (the overscan being extra readouts of the serial register after the last row of the image has been read out) is necessary. However, columns affected by hot pixels and saturated sources may bleed into the parallel overscan region, requiring them to be masked and interpolated along the columns. Additionally, these high signals induce electronic crosstalk (see section 2.7 below) into overscan regions of other amplifiers, necessitating crosstalk correction of the overscan region. Following these corrections, the ISR task performs the column-by-column parallel overscan correction.

2.6 Linearity correction

Signal-chain non-linearity in the LSSTCam detectors¹² is corrected per amplifier, and the correction is derived from a dataset used to calculate the PTC: a set of flat-field images (flat pairs) at different flux levels, monitored by a photodiode. All non-linearity corrections are defined in terms of an additive correction, such that:

$$\text{corrected value} = \text{uncorrected value} + f(\text{uncorrected value})$$

There are currently multiple options for the correction function f , including a lookup table, a polynomial function in which a polynomial is used to approximate the inverse of the response function,¹³ and a spline fit. The current configuration file for LSSTCam employs a multi-node spline⁴.

2.7 Correction of the crosstalk between amplifiers

Crosstalk in LSSTCam detectors refers to the phenomenon where a signal from one amplifier “leaks” into another. This is a significant concern due to the highly parallelized readout of LSST’s focal plane, which is designed to read out 3.2 Gpixels in 2 seconds, resulting in a total of 3024 synchronously read-out video channels (16 channels or amplifiers per detector). The unique combination of high speed, high-resistivity silicon, low power, and close channel spacing makes the LSST readout more prone to electronic crosstalk than previous mosaic cameras. The primary source of crosstalk is capacitive coupling between single-ended video outputs from the CCD, which can occur both within a single CCD and between CCDs in the focal plane. This interference can also originate from the readout electronics themselves.¹⁴ To correct this, a comprehensive matrix for each detector is required, detailing the effect of each source amplifier on every target amplifier. It’s anticipated that crosstalk between CCDs will be less than intra-CCD crosstalk, with inter-raft crosstalk being negligible. Interestingly, the LSSTCam also shows a unique form of crosstalk between CCD amplifier segments that does not linearly scale with intensity, differing from what would be expected from capacitive coupling alone.¹⁵

2.8 Bias subtraction, using a combined bias frame

A 2D combined bias frame (commonly referred to in the LSST Science Pipelines as simply a “bias” frame) must be subtracted during ISR. This frame represents the signal recorded by the CCD when

⁴As proposed by P. Astier (LPNH, (IN2P3/CNRS))

no light is present and with no integration time, including the inherent electronic noise of the CCD and the readout system, as well as any other systematic effects present even when no light is hitting the detector. To construct a combined bias frame, a series of individual biases (typically ≈ 20 to minimize the noise in the combined bias frame¹⁶) or exposures at zero integration time are taken as input. The overscan, crosstalk, and assembly steps previously discussed are applied to the input zero-second exposure time images, which are then combined using a clipped per-pixel mean (i.e., an iteratively sigma-clipped mean is computed on the set of individual bias images) to construct the output bias correction. Crosstalk correction must be performed before bias frame creation to ensure that the crosstalk signal from hot columns is corrected. Otherwise, these signals will imprint on all of the amplifier segments in subsequent detrending steps.

2.9 *Gain scaling**

The process of converting the units of each amplifier from ADU to e^- using the gain measurement involves two steps.¹¹ Initially, the image is corrected to account for the slight dependence of the gain on the temperature of the readout electronics board (REB) controlling it (approximately 0.06%/C). This correction is necessary to accommodate any minor temperature shifts and ensure all images can use equivalent calibrations. In the second step, the gains (e^-/ADU) are used to convert each amplifier from ADU units to e^- units. After the temperature shifts have been corrected, the PTC analysis is used to measure the gain from each amplifier. The current PTC pipeline in the LSST Science Pipelines takes as input a series of raw flat pairs at different fluxes and has 3 main steps: “ISR”, where instrument-signature removal is applied; “extract”, where the covariances from flats up to a certain lag (with a default value of 8) using the Fast Fourier Transform algorithm from Appendix A in Astier et al. (2019)¹⁷ are measured; and “Solve”, where the measured covariances are fitted to models described in Astier et al. (2019)¹⁷ (the models in Equations 16 and 20 of that paper).

2.10 *Charge-Transfer Inefficiency (CTI) correction*

CTI is the phenomenon where the voltage changes that serve to shift the photoelectrons toward the readout amplifiers do so incompletely, resulting in charge that becomes trapped in the silicon. When this charge is released later, it manifests visually as spurious trails behind every source object. This trailing caused by CTI is particularly problematic as the amount of flux trailed has a nonlinear relationship with the flux and size of the source and the recent illumination history of the detector. CTI differs between the serial and parallel transfer readout directions due to their distinct charge transfer methods and spacings of wells.¹⁸ The LSST Science Pipelines implement a detector and segment-dependent CTI correction algorithm described by Snyder et al. (2020)¹⁹ to correct for serial CTI in ITL devices. This algorithm aims to accurately model and account for the position- and flux-dependent nature of CTI trailing seen in LSST images.

2.11 *Amplifier assembly and trimming*

The overscan regions of the images are trimmed, and the 16 amplifiers per detector are assembled into a single CCD image.

2.12 Variance calculation (variance image construction)

A weight map is calculated from assembled and trimmed images based on the measured variance per pixel. This is constructed by first dividing each image segment by the gain (e^-/ADU) of that segment to derive the Poisson variance, and then adding the square of the read noise to derive a map of the empirical uncertainty across an image (the “Variance Plane Image”). The read noise can be measured empirically from the overscan region of the detector and can also be calculated as a parameter from the fit to the PTC.

2.13 Defect mask interpolation

Defects are determined as the outliers of the pixel value distributions from dark and flat-field images and are set to the BAD flag. Individual or combined darks and flats can be used. The thresholds in darks and flats can be specified in terms of values or standard deviations from the mean.

2.14 Dark subtraction, using a combined dark frame

A combined dark image, to be subtracted from science images, is constructed by taking a clipped per-pixel mean from a set of individual dark images, similar to the bias image described in section 2.8. Individual dark images of the entire LSSTCam focal plane are captured with the camera shutter closed, including contributions from dark current and light leakages. Dark images are also used to create defect maps and are taken at different integration times to study dynamic defects or bad columns.

2.15 Brighter-fatter effect correction

The brighter-fatter effect (BFE) refers to the observed growth in the sizes of stars with signal level, resulting from the deflection of in-falling charges by transverse electric fields produced by already accumulated charges in the potential wells of pixels.²⁰⁻²³ The BFE leads to correlations between pixels and is calibrated from measured pixel correlations in flat fields, as it smooths out Poisson noise fluctuations at high signal levels. The strength of the BFE can differ along the channel stops or barrier clock gates in a sensor, it can vary mildly with color, and its impact on pixel correlations does not necessarily scale linearly with signal level.

The effect is calibrated from the empirical correlations in the limit of zero signal, at a user-specified signal level, or an average of correlations across a range of signal levels. The pixel correlations are derived from the flat-field image covariances measured out to a lag of 8 pixels, as mentioned in section 2.9. Fully capturing the range of the effect is important for the correction to conserve charge. To verify this, the sum of the pixel correlations out to this distance is checked for consistency with zero. A PTC with at least 1000 points from near zero signal up to saturation is necessary to constrain the anisotropy, magnitude, and range of the effect, as well as the evolution of the strength of the BFE with signal level. When the measurement of correlations at large distances is limited by statistical fluctuations, an empirically measured power law is used to project the pixel correlations out to larger distances.

The BFE is corrected under the assumption that the derived pixel correlations are proportional to the Laplacian of a constant, unitless, 2-dimensional, scalar kernel, which is assumed to represent the displacement field due to a single accumulated charge.^{12,24} This kernel is then convolved with

the measured image to recover a template representing the amount of displaced charge due to the BFE. This template is subsequently added to the measured image to recover the true image. The kernel is applied recursively until the amount of shifted charge at each iteration falls below a threshold of 1000 electrons across the whole image. If the kernel accurately models the effect, no more than 2–3 iterations should be required to converge to a solution.

The BFE can empirically vary from amplifier to amplifier or sensor to sensor and mildly from wavelength to wavelength. Therefore, calibrations are derived for each sensor, amplifier, and filter band. However, to avoid discontinuities along amplifier boundaries, the 16 kernels for each channel of a given sensor are averaged to create a single detector-level kernel that is ultimately used to remove the effect from images taken by that sensor. Ultimately, we apply one calibrated kernel per sensor per filter band.

The BFE is small, and the calibration of the BFE can be sensitive to gain estimation as well as the calibration of other artifacts that affect the measured pixel correlations, such as charge transfer inefficiency (CTI), signal-chain non-linearity, overscan subtraction, as well as other sensor-specific calibrations. Since the BFE is one of the first instrument signatures to impact an exposure, the correction must be applied near the end of the ISR pipeline. Extreme care must therefore be taken to remove these other effects and validate these other ISR steps before deriving calibrations for the BFE from flat fields and applying the correction to an image.

The kernel is initially validated by backward-correcting flat images to linearize the PTC, as a good-quality kernel should be able to recover the Poisson noise in the flat field images. In general, the sub-pixel electric fields inside a flat image do not approximate the sub-pixel electric fields inside a typical science image, and the slope of the second moment vs. magnitude of stellar sources is also checked to be consistent with zero.^{12,23,25}

2.16 Flat-field corrections to convert image to units of fluence*

After the previous correction steps have been applied, an unflattened, gain-scaled `post-ISR` image in e^- with instrument signatures removed is obtained. Flat fielding is incorporated into the subsequent photometric calibration process, which aims to estimate the surface brightnesses of celestial sources uniformly across the sky as would be measured at the top of the Earth's atmosphere.^{11,26,27} This process involves constructing a “background flat” per filter for image background subtraction using monochromatic dome flats and sky data (including background template estimation via, *e.g.*, Principal Component Analysis²⁶), along with a “reference flux flat” per filter and as described in Bernstein et al. (2017).²⁶ The reference flux flat measures the response to focused light and differs from a dome flat in several respects, including accounting for pixel size variations by removing the effects of transverse electric fields (*e.g.*, tree rings^{28–30} and edge distortions or “picture frames”^{31,32}), and accounting for differences in focused and scattered light patterns from flat-field screens and sky sources, and contamination by scattered light.¹¹

After this flat-fielding process (including fringe⁵ correction for redder bands³³), a fluence image in e^- is obtained, as depicted in the lower right steps of the flow chart in Figure 2. The subsequent process of turning this fluence image into a Processed Visit Image in physical units (nJy) involves the construction of a point-spread function model, morphological cosmic-ray finding and masking, and the construction of astrometric³⁴ and photometric solutions²⁷ (see, *e.g.*, Bosch et al. 2018⁸ for

⁵Fringing arises from interference effects as light passes through and reflects within the layers of the CCD and its coatings/filters.

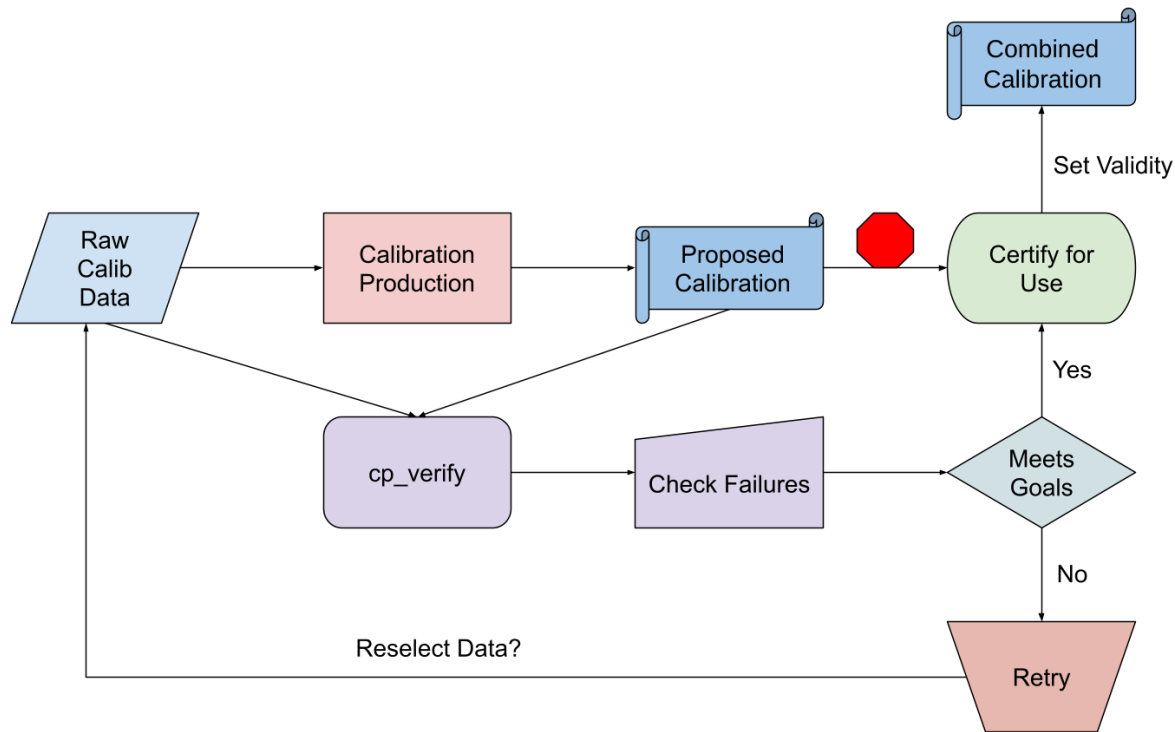


Fig 3 Calibration flow chart. Credit: Chris Waters, Data Management Technical Note 222³⁵

a description of this process in the context of the Hyper Supreme-Cam survey using a previous version of the LSST Science Pipelines).

3 Calibration Products Production for ISR

Calibration products are required to carry out the ISR steps. To validate a new combined calibration for use, metrics are measured on a residual image that results after applying a given calibration (e.g., a bias-subtracted individual bias) and compared to expectations and limits (using a series of tests and metrics defined in the Data Management Technical Note 101,¹⁶ see Table 1). This is accomplished via the `cp_verify` package.⁶ If all metrics are within limits, the calibration is certified for a date range during which it will be used, though the end date may be unknown.

⁶https://github.com/lsst/cp_verify

Calibration products	Verification criteria
Bias and Dark	<ul style="list-style-type: none"> • Mean consistent with zero. • Clipped standard deviation consistent with read noise. • Cosmic rays rejected standard deviation consistent with read noise.
Brighter-fatter correction	<ul style="list-style-type: none"> • Slope of source second-moment size as a function of source magnitude small ($\lesssim 1\%$).

Table 1 Examples of `cp_verify` tests for calibration verification. Bias: using bias-corrected individual bias exposures. Dark: using bias- and dark-corrected individual dark exposures. Brighter-fatter correction: using full ISR-processed science exposures.

These validations are also used with daily calibrations to monitor the stability of the camera and telescope by confirming that existing combined calibrations remain suitable. Figure 3 shows the relationship between construction, validation, and usage of combined calibrations. It can be summarized as:

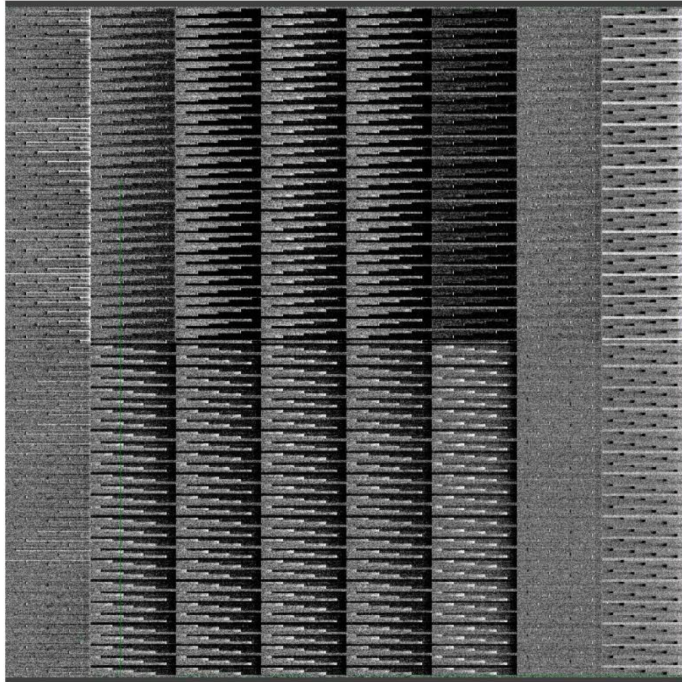
- A proposed calibration is constructed,
- `cp_verify` tasks check that it meets verification metrics,
- If the tests pass, the calibration can be certified by a Calibration Acceptance Board, assigned a validity range, and deployed as a standard calibration.

Figure 4 shows an example of a defective bias failing the tests defined in `cp_verify`.

4 The LSST Data Butler, Calibration Collections, and Calibration Pipelines

The Rubin data management system uses a “data Butler” to organize and locate datasets.³⁶ This Butler groups data into “collections,” with a special “calibration collection” that associates calibration datasets with a validity time range. When image processing is started, the Butler uses these validity time ranges to match the supplied calibration data to the images to be processed. Calibrations that are not calculated from available data (like quantum efficiency curves) or are relatively static (like defect masks) are called “curated calibrations.” These are stored in text files in GitHub repositories with a directory structure that encodes their validity ranges⁷. Processing is done via `PipelineTasks`. Each `PipelineTask` provides one processing step, and several can be combined into a full pipeline defined in a YAML file. Figure 5 shows a diagram depicting the `PipelineTasks` involved in the creation of a combined bias using the bias pipeline. The *dimensions* are the key variables or parameters that define the characteristics of a Butler dataset,

⁷For example, https://github.com/lsst/obs_lsst_data/tree/main/lsstCam stores transmission curves for LSSTCam



Exposure	Detector	NOISE	MEAN
2021081900004	R22_S00	14	1
2021081900003	R22_S00	16	10
2021080500003	R22_S00	3	0

Fig 4 `cp_verify` identifying a defective combined bias from a particular detector due to an acquisition problem, as indicated in the “failure table” in the right, using the tests of Table 1: NOISE corresponds to “Clipped standard deviation consistent with read noise” and MEAN corresponds to “Mean consistent with zero”.

such as its observation time, instrument configuration, target coordinates, filter, etc., that allow it to be uniquely identified and located within the data archive system.³⁶ The `ISR PipelineTasks` for LSSTCam provide the functionality to remove systematic errors from the raw instrument data, using the calibration products discussed above. Multiple `ISR PipelineTasks` with different configurations can be defined to handle different instruments.

Disclosures

There are no conflicts of interest.

Code, Data, and Materials Availability

The LSST Science Pipelines (pipelines.lsst.io) code described in this article is open-source and available in the following repositories: https://github.com/lsst/ip_isr, https://github.com/lsst/cp_pipe, and https://github.com/lsst/cp_verify.

Acknowledgments

The work of AAPM was supported by the U.S. Department of Energy under contract number DE-AC02-76SF00515. This paper makes use of LSST Science Pipelines software developed by the Vera C. Rubin Observatory. We thank the Rubin Observatory for making their code available as free software at <https://pipelines.lsst.io>. This material or work is supported in part by the National Science Foundation through Cooperative Agreement AST-1258333 and Cooperative Support Agreement AST1836783 managed by the Association of Universities for Research in Astronomy (AURA), and the Department of Energy under Contract No. DE-AC02-76SF00515

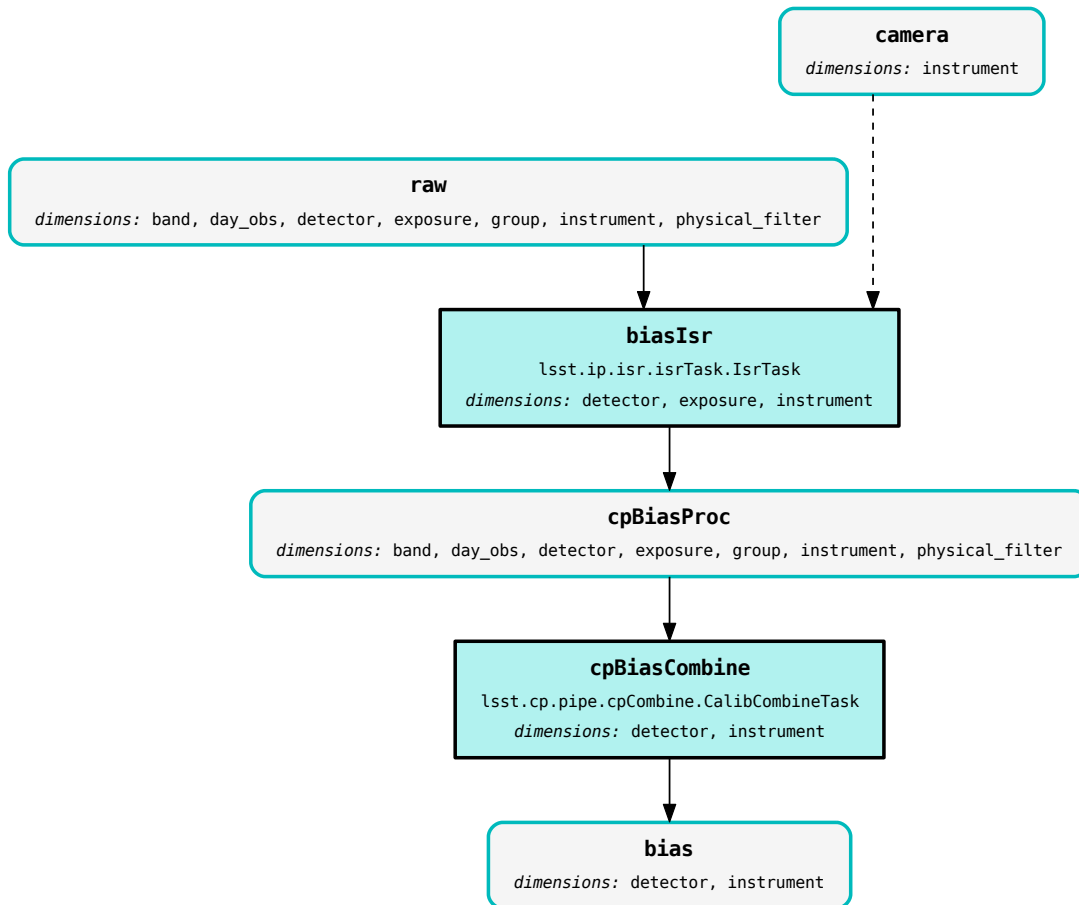


Fig 5 PipelineTasks in the bias pipeline to produce a combined bias. Diagram credit: L. Kelvin and the LSST Science Pipelines.

with the SLAC National Accelerator Laboratory managed by Stanford University. AAPM thanks the Department of Physics of Harvard University and the Laboratory of Particle Astrophysics and Cosmology led by Prof. Chris Stubbs for their hospitality during the preparation of this paper. We thank S. Digel (SLAC National Accelerator Laboratory) for serving as Rubin’s internal reviewer and providing comments that improved the manuscript. We thank T. Jenness (Rubin) and Z. Ivezic (Rubin, University of Washington) for providing comments that improved the manuscript.

References

1. Ivezic, S. M. Kahn, J. A. Tyson, *et al.*, “LSST: From science drivers to reference design and anticipated data products,” *The Astrophysical Journal* **873**, 111 (2019).
2. S. E. Holland, D. E. Groom, N. P. Palaio, *et al.*, “Fully depleted, back-illuminated charge-coupled devices fabricated on high-resistivity silicon,” *IEEE Transactions on Electron Devices* **50**, 225–238 (2003).
3. S. E. Holland, W. F. Kolbe, and C. J. Bebek, “Device Design for a 12.3-Megapixel, Fully Depleted, Back-Illuminated, High-Voltage Compatible Charge-Coupled Device,” *IEEE Transactions on Electron Devices* **56**, 2612–2622 (2009).
4. S. E. Holland, C. J. Bebek, W. F. Kolbe, *et al.*, “Physics of fully depleted CCDs,” *Journal of Instrumentation* **9**, C03057 (2014).
5. P. O’Connor, P. Antilogus, P. Doherty, *et al.*, “Integrated system tests of the LSST raft tower modules,” in *High Energy, Optical, and Infrared Detectors for Astronomy VII*, A. D. Holland and J. Beletic, Eds., *Society of Photo-Optical Instrumentation Engineers (SPIE) Conference Series* **9915**, 99150X (2016).
6. K. Arndt, V. Riot, E. Alagoz, *et al.*, “The LSST camera corner raft conceptual design: a front-end for guiding and wavefront sensing,” in *Adaptive Optics Systems II*, B. L. Ellerbroek, M. Hart, N. Hubin, *et al.*, Eds., *Society of Photo-Optical Instrumentation Engineers (SPIE) Conference Series* **7736**, 773662 (2010).
7. M. Lesser and D. Ouellette, “Results from STA/ITL fully depleted CCDs for LSST,” *Journal of Instrumentation* **12**, C03080 (2017).
8. J. Bosch, R. Armstrong, S. Bickerton, *et al.*, “The Hyper Suprime-Cam software pipeline,” *Publications of the Astronomical Society of Japan* **70**, S5 (2018).
9. J. Bosch, Y. AlSayyad, R. Armstrong, *et al.*, “An Overview of the LSST Image Processing Pipelines,” in *Astronomical Data Analysis Software and Systems XXVII*, P. J. Teuben, M. W. Pound, B. A. Thomas, *et al.*, Eds., *Astronomical Society of the Pacific Conference Series* **523**, 521 (2019).
10. J. R. Janesick, *Scientific charge-coupled devices*, SPIE, Bellingham (2001).
11. P. Fagrelus and E. Rykoff, “Rubin Baseline Calibration Plan,” (2023). Vera C. Rubin Observatory Commissioning Technical Note SITCOMTN-086.
12. C. Lage, “Linearity and correction of the BF effect in LSST sensors,” *arXiv e-prints*, arXiv:1911.09567 (2019).
13. J. K. C. Freudenburg, J. J. Givans, A. Choi, *et al.*, “Brighter-fatter Effect in Near-infrared Detectors—III. Fourier-domain Treatment of Flat Field Correlations and Application to WFIRST,” *PASP* **132**, 074504 (2020).
14. P. O’Connor, “Crosstalk in multi-output CCDs for LSST,” *Journal of Instrumentation* **10**, C05010 (2015).

- 15 A. Snyder, A. Barrau, A. Bradshaw, *et al.*, “Laboratory Measurements of Instrumental Signatures of the LSST Camera Focal Plane,” *arXiv e-prints* , arXiv:2101.01281 (2021).
- 16 Lupton, R. and Plazas Malagón, A., “Verifying LSST Calibration Data Products,” (2018). Vera C. Rubin Observatory Data Management Technical Note DMTN-101.
- 17 P. Astier, P. Antilogus, C. Juramy, *et al.*, “The shape of the photon transfer curve of CCD sensors,” *AAP* **629**, A36 (2019).
- 18 R. Massey, T. Schrabback, O. Cordes, *et al.*, “An improved model of charge transfer inefficiency and correction algorithm for the Hubble Space Telescope,” *Monthly Notices of the Royal Astronomical Society* **439**, 887–907 (2014).
- 19 A. Snyder and A. Roodman, “Investigation of Deferred Charge Effects in LSST ITL Sensors,” *arXiv e-prints* , arXiv:2001.03223 (2020).
- 20 P. Antilogus, P. Astier, P. Doherty, *et al.*, “The brighter-fatter effect and pixel correlations in ccd sensors,” *Journal of Instrumentation* **9**, C03048C03048 (2014).
- 21 A. Guyonnet, P. Astier, P. Antilogus, *et al.*, “Evidence for self-interaction of charge distribution in charge-coupled devices,” *AAP* **575**, A41 (2015).
- 22 D. Gruen, G. M. Bernstein, M. Jarvis, *et al.*, “Characterization and correction of charge-induced pixel shifts in DECam,” *Journal of Instrumentation* **10**, C05032 (2015).
- 23 A. Broughton, Y. Utsumi, A. Plazas Malagón, *et al.*, “Mitigation of the Brighter-Fatter Effect in the LSST Camera,” *arXiv e-prints* , arXiv:2312.03115 (2023).
- 24 W. R. Coulton, R. Armstrong, K. M. Smith, *et al.*, “Exploring the Brighter-fatter Effect with the Hyper Suprime-Cam,” *Astronomical Journal* **155**, 258 (2018).
- 25 P. Astier and N. Regnault, “Correction of the brighter-fatter effect on the CCDs of Hyper Suprime-Cam,” *Astronomy and Astrophysics* **670**, A118 (2023).
- 26 G. M. Bernstein, T. M. C. Abbott, S. Desai, *et al.*, “Instrumental response model and detrending for the Dark Energy Camera,” *Publications of the Astronomical Society of the Pacific* **129**, 114502 (2017).
- 27 G. M. Bernstein, T. M. C. Abbott, R. Armstrong, *et al.*, “Photometric Characterization of the Dark Energy Camera,” *Publications of the Astronomical Society of the Pacific* **130**, 054501 (2018).
- 28 A. A. Plazas, G. M. Bernstein, and E. S. Sheldon, “On-Sky Measurements of the Transverse Electric Fields’ Effects in the Dark Energy Camera CCDs,” *Publications of the Astronomical Society of the Pacific* **126**, 750–760 (2014).
- 29 H. Y. Park, A. Nomerotski, and D. Tsybychev, “Properties of tree rings in LSST sensors,” *Journal of Instrumentation* **12**, C05015 (2017).
- 30 J. H. Esteves, Y. Utsumi, A. Snyder, *et al.*, “Photometry, Centroid and Point-spread Function Measurements in the LSST Camera Focal Plane Using Artificial Stars,” *Publications of the Astronomical Society of the Pacific* **135**, 115003 (2023).
- 31 A. A. Plazas, G. M. Bernstein, and E. S. Sheldon, “Transverse electric fields’ effects in the Dark Energy Camera CCDs,” *Journal of Instrumentation* **9**, C04001 (2014).
- 32 A. A. Plazas Malagn, “Transverse electric fields effects in decam devices: tree rings and glowing edges,” *Precision Astronomy with Fully-Depleted CCDs (PACCDs)*, Brookhaven National Laboratory, November, 2013, Zenodo, DOI: 10.5281/zenodo.10064122 (2013).

- 33 Z. Guo, C. W. Walter, C. Lage, *et al.*, “Fringing Analysis and Simulation for the Vera C. Rubin Observatory’s Legacy Survey of Space and Time,” *Publications of the Astronomical Society of the Pacific* **135**, 034503 (2023).
- 34 G. M. Bernstein, R. Armstrong, A. A. Plazas, *et al.*, “Astrometric Calibration and Performance of the Dark Energy Camera,” *Publications of the Astronomical Society of the Pacific* **129**, 074503 (2017).
- 35 C. Waters, “Calibration Generation, Verification, Acceptance, and Certification.,” (2023). Vera C. Rubin Observatory Data Management Technical Note DMTN-222.
- 36 T. Jenness, J. F. Bosch, A. Salnikov, *et al.*, “The Vera C. Rubin Observatory Data Butler and pipeline execution system,” in *Software and Cyberinfrastructure for Astronomy VII, Society of Photo-Optical Instrumentation Engineers (SPIE) Conference Series* **12189**, 1218911 (2022).

List of Figures

- 1 Example of an image before and after partial Instrument Signature Removal (bias, dark, and flat applied).
- 2 ISR steps and necessary calibration products. Units are displayed in each box, and the steps in red and enclosed in dashed lines are in the process of being implemented. Flowchart based on discussions at Rubin Calibration Workshop at SLAC, October 2023.
- 3 Calibration flow chart. Credit: Chris Waters, Data Management Technical Note 222³⁵
- 4 `cp_verify` identifying a defective combined bias from a particular detector due to an acquisition problem, as indicated in the “failure table” in the right, using the tests of Table 1: NOISE corresponds to “Clipped standard deviation consistent with read noise” and MEAN corresponds to “Mean consistent with zero”.
- 5 `PipelineTasks` in the bias pipeline to produce a combined bias. Diagram credit: L. Kelvin and the LSST Science Pipelines.

List of Tables

- 1 Examples of `cp_verify` tests for calibration verification. Bias: using bias-corrected individual bias exposures. Dark: using bias- and dark-corrected individual dark exposures. Brighter-fatter correction: using full ISR-processed science exposures.